Journal of the Korean Nuclear Society
Volume 36, Number 4, pp.248~262, June, 2004

Assessment of RANS Models for 3-D Flow Analysis of SMART

Kun Ho Chun, Young Dong Hwang, Han Young Yoon,
Hee Chul Kim, and Sung Quun Zee
Korea Atomic Energy Research Institute
150 Deokjin-dong, Yuseong-gu, Daejeon 305-353, Korea
ex-khchun@kaeri.re.kr

(Received October 29, 2003)

Abstract

Turbulence models are separately assessed for a three dimensional thermal-hydraulic analysis of the integral reactor SMART. Seven models (mixing length, k-l, standard k-ε, k-ε-fμ, k-ε-v2, RRSM, and ERRSM) are investigated for flat plate channel flow, rotating channel flow, and square sectioned U-bend duct flow. The results of these models are compared to the DNS data and experiment data. The results are assessed in terms of many aspects such as economical efficiency, accuracy, theorization, and applicability. The standard k-ε model (high Reynolds model), the k-ε-v2 model, and the ERRSM (low Reynolds models) are selected from the assessment results. The standard k-ε model using small grid numbers predicts the channel flow with higher accuracy in comparison with the other eddy viscosity models in the logarithmic layer. The elliptic-relaxation type models, k-ε-v2, and ERRSM have the advantage of application to complex geometries and show good prediction for near wall flows.

Key Words : SMART primary coolant system, turbulence model, eddy viscosity model, reynolds stress model, elliptic relaxation method, damping function

1. Introduction

The flow of a SMART primary coolant system is a strong inhomogeneous turbulent flow combined with forced and natural convections. The structure of the SMART primary coolant system consists of complex geometry including multi-walls, multi-blocks, strong streamline curvatures, and variable-cross-sections. The down-comer region of SMART, which consists of shielding materials and a core region, may develop a locally stagnant coolant flow [1,2]. Since this flow field depends strongly on the adopted turbulence model, the selection of an appropriate turbulence model for the flow analysis is very important.

The turbulence models used in computational fluid dynamics can be divided into three categories: RANS (Reynolds Averaged Navier Stokes), LES (Large Eddy Simulation), and DNS (Direct Numerical Simulation). Although LES and DNS yield better predictions than RANS, this study is limited to RANS models, which give good predictions with small numbers of computational grids. The RANS models used are mixing length

[3,4], k-l [5], k-ε [6], k-ε-fμ [7], and k-ε-v2 [8], as well as the Reynolds stress models (Speziale, Sarkar, and Gatski [9] and Durbin' s elliptic relaxation method [10]).

The mixing length model uses an explicit algebraic approximation for the velocity scale and the length scale of the eddy viscosity. However, the eddy viscosity of the standard k-ε and k-ε-fμ models was calculated using two differential equations (i.e., k and ε transport equations). Here, fμ is the explicitly calculated damping function. The k-ε-v2 model also includes the $\overline{v^2}$-equation in addition to the k and ε equations. The three types of k-ε models have computational advantages of simplicity and stability in modeling despite the need to solve partial differential equations. These models assume isotropic eddy viscosity, allowing them to be simply incorporated into any existing computer code developed to solve the laminar Navier-Stokes equations.

The Reynolds stress models (RSM) have not been as widely used in engineering applications as the eddy viscosity models. However, RSMs are regarded as the natural and most logical approach among the RANS models, since RSMs provide an extra turbulent momentum flux from the solution of full transport equations. These models have received much attention with regard to investigation of isotropy/anisotropy effects and the homogeneous/non-homogeneous turbulences. RSMs also require more computational resources than the eddy viscosity model in order to solve the components of the Reynolds stress transport equations.

The present study assesses the turbulence models that will be implemented into TASS-3D, the three-dimensional thermal-hydraulic analysis computer code of SMART. Three flow fields, the flat plate channel, rotating channel, and U-bend duct, are investigated to assess the models. The results are evaluated for applicability, accuracy, theorization, and economical efficiency with consideration of the specific flow characteristics of the SMART primary coolant system.

2. Governing Equations and RANS Models

The following seven RANS models were investigated for application to a three-dimensional flow analysis of the SMART primary coolant system. These models have been theoretically verified and are widely used in industrial applications.

(1) Mixing length model: Van Driest [3], Escudier [4]
(2) k-l model: Wolfstein [5]
(3) Standard k-ε model: Launder and Spalding [6]
(4) k-ε-fμ model: Launder and Sharma [7]
(5) k-ε-v2 model: Durbin [8]
(6) Realizable RSM: Speziale, Sarkar and Gatski [9]
(7) Elliptic Relaxation RSM: Durbin [10]

The governing equations, wall corrections (or damping functions) and model constants of these models are summarized in Tables 1 and 2. Among them, the mixing length and k-ε models are the most widely used and validated. These models are derived based on the assumption that there exists an analogy between the action of the viscous stress and the Reynolds stress on the mean flow. Prandtl postulated that for flows near solid boundaries the mixing length is proportional to the distance from the surface. This postulation is consistent with the well known law of the wall, which has been observed for a wide range of wall bounded flows. Van Direst [3] proposed a modified model wherein the mixing length is multiplied by a damping function. Specifically, Van Direst suggested that in the near-wall layer the mixing length behaves as delineated in Table 2.

Table 1. Governing Equations and Turbulence Models

• Momentum equation

$$\frac{\partial(\rho u_i)}{\partial t}+\frac{\partial(\rho u_i u_j)}{\partial x_j}=-\frac{\partial p}{\partial x_i}+\frac{\partial}{\partial x_j}\left(\mu\frac{\partial u_i}{\partial x_j}-\overline{u_i u_j}\right)-2\Omega_j U_k e_{ijk} \tag{1}$$

• k and ε equations

$$\frac{\partial k}{\partial t}+\frac{\partial u_j k}{\partial x_j}=P_k-\epsilon+\frac{\partial}{\partial x_j}\left[(\nu+\frac{\nu_T}{\sigma_k})\frac{\partial k}{\partial x_j}\right] \tag{2}$$

$$\frac{\partial \epsilon}{\partial t}+\frac{\partial u_i \epsilon}{\partial x_j}=C_{\epsilon 1}f_1\frac{P\epsilon}{k}-C_{\epsilon 2}f_2\frac{\epsilon^2}{k}+\frac{\partial}{\partial x_k}\left[(\nu+\frac{\nu_T}{\sigma_\epsilon})\frac{\partial \epsilon}{\partial x_k}\right] \tag{3}$$

• Eddy viscosity model

$$-\rho\overline{u_i u_j}=\rho\nu_T\left(\frac{\partial u_i}{\partial x_j}+\frac{\partial u_j}{\partial x_i}\right)-\frac{2}{3}k\delta_{ij} \tag{4}$$

• Reynolds stress equations

$$\frac{D\overline{u_i u_j}}{Dt}=P_{ij}+\Phi_{ij}+D^v_{ij}+D^t_{ij}+D^p_{ij}-\epsilon_{ij}+R_{ij} \tag{5}$$

$$P_{ij}=-\left(\overline{u_k u_i}\frac{\partial U_j}{\partial x_k}+\overline{u_k u_j}\frac{\partial U_i}{\partial x_k}\right) \tag{5a}$$

$$R_{ij}=-2\Omega_k\left(\overline{u_j u_m}e_{ikm}+\overline{u_i u_m}e_{jkm}\right) \tag{5b}$$

$$D^\nu_{ij}=\frac{\partial}{\partial x_k}\left(\nu\frac{\partial\overline{u_i u_j}}{\partial x_k}\right) \tag{5c}$$

$$D^t_{ij}+D^p_{ij}=-\frac{\partial}{\partial x_k}\left(\overline{u_i u_j u_k}+\left(\frac{\overline{pu_i}}{\rho}\delta_{jk}+\frac{\overline{pu_j}}{\rho}\delta_{ik}\right)\right)=\frac{\partial}{\partial x_k}\left(C_k\overline{u_l u_m}T\frac{\partial\overline{u_i u_j}}{\partial x_m}\right) \tag{5d}$$

$$\epsilon_{ij}=2\nu\frac{\partial u_i}{\partial x_k}\frac{\partial u_j}{\partial x_k}=\frac{\overline{u_i u_j}}{k}\epsilon \tag{5e}$$

• Pressure strain model(SSG)

$$\Phi_{ij}=\alpha_1\epsilon b_{ij}+\alpha_2\epsilon(b_{ik}b_{kj}-\frac{1}{3}b_{kl}b_{kl}\delta_{ij}) \tag{6}$$
$$+\alpha_3 P_k b_{ij}+\alpha_4 k S_{ij}+\alpha_5 k(b_{ik}S_{jk}+b_{jk}S_{ik}-2/3 b_{kl}S_{kl}\delta_{ij})+\alpha_6 k(b_{ik}W_{jk}+b_{jk}W_{ik})$$

$$b_{ij}=\frac{\overline{u_i u_j}}{2k}-\frac{1}{3}\delta_{ij},\ P_k=\overline{u_i u_j}\frac{\partial u_i}{\partial x_j},\ S_{ij}=\frac{1}{2}\left(\frac{\partial u_i}{\partial x_j}+\frac{\partial u_j}{\partial x_i}\right),\ W_{ij}=\frac{1}{2}\left(\frac{\partial u_i}{\partial x_j}-\frac{\partial u_j}{\partial x_i}\right)+e_{mji}\Omega_m$$

• Elliptic relaxation model

$$f_{ij}-L^2\nabla^2 f_{ij}=\frac{F_{ij}}{k},\ \Phi_{ij}=kf_{ij} \tag{7}$$

$$F_{ij}=\Phi_{ij}+\frac{\overline{u_i u_j}}{k}\epsilon-\frac{2}{3}\epsilon\delta_{ij} \tag{8}$$

Table 2. Eddy Viscosity, Wall Functions and Model Coefficients for the Turbulent Models

Model	ν_T	Wall correction	Model constant
mixing length	$l_{mix}^2\left\|\frac{dU}{dy}\right\|$	$l_{mix} = f(y^+, \delta)$	$l_{mix}^{inner} = \kappa y[1 - exp(-y^+/26)]$ $l_{mix}^{outer} = max(l_{mix}, 0.09\delta),\ y^+ = \frac{y\delta}{\nu}$
k-l	$C_\mu\sqrt{k}l_\mu$	$l_\mu = C_1 y\left[1 - \exp\left(-\frac{R_y}{A_\mu}\right)\right]$	$C_1 = \kappa C_\mu^{-3/4},\ R_y = \sqrt{k}y/\nu$ $A_\mu = 70.0,\ \kappa = 0.41$
k-ε	$C_\mu k^2/\epsilon$	$U^+ = (1/\kappa)\ln(Ey^+)$	$E = 9.8,\ \kappa = 0.41,\ C_\mu = 0.09$
k-ε-fμ	$C_\mu f_\mu k^2/\epsilon$	$f_\mu = f(R_T, y^+)$	$f_\mu = \exp\left[-3.4/(1 + \frac{R_T}{50})\right],\ R_T = \frac{k^2}{\nu\epsilon}$ $f_1 = 1, f_2 = 1 - 0.3\exp(-R_T^2),\ C_\mu = 0.09$
k-ε-v2	$C_\mu \overline{v^2} k/\epsilon$	$f_{22} - L^2\nabla^2 f_{22} = \frac{F_{22}}{k}$	$L = C_L\max\left(\frac{k^{3/2}}{\epsilon}, 70\left(\frac{\nu^3}{\epsilon}\right)^{1/4}\right)$, $T = \max\left(\frac{k}{\epsilon}, C_T\left(\frac{\nu}{\epsilon}\right)^{1/2}\right)$, $C_L = 0.3,\ C_T = 6.0,\ C_\mu = 0.22$
RSM	*RRSM*	$\alpha_i = f(A, B_2)$	$\alpha_1 = -3.4, \alpha_2 = 4.2, \alpha_3 = -1.8$ $\alpha_4 = 0.8 - 1.3B_2^{1/2}, \alpha_5 = 1.2, \alpha_6 = 0.4$ $B_2 = b_{ij}b_{ji}$
	ERRSM	$f_{ij} - L^2\nabla^2 f_{ij} = \frac{F_{ij}}{k}$	$L = C_L\max\left(\frac{k^{3/2}}{\epsilon}, 80\left(\frac{\nu^3}{\epsilon}\right)^{1/4}\right), C_L = 0.2$ $T = \max\left(\frac{k}{\epsilon}, C_T\left(\frac{\nu}{\epsilon}\right)^{1/2}\right), C_T = 6.0$

Escudier [4] found that the predictive accuracy is improved by limiting the peak value of the mixing length according to Table 2. This model includes the damping function in the inner layer and outer layer, as shown in Table 2. The k-l model proposed by Wolfstein [5] calculates the k-transport equation instead of the velocity scale.

The standard k-ε model is the simplest complete model of the RANS turbulence models, for which only the boundary conditions need to be supplied. However, this model needs strong corrections for a solid boundary. In order to avoid this weakness, the k-ε-fμ model is derived by introducing damping functions to account for the effect of the wall on the turbulence. The function fμ corrects the strong overestimation of the turbulent viscosity in the vicinity of the wall, but these functions frequently cause numerical stiffness and poor predictions in complex flows.

In contrast to this approach, Durbin [8] suggested replacing the turbulent kinetic energy with the velocity scale ($\overline{v^2}$) in the eddy viscosity, since the primary objective of introducing the damping effect to the closure models is to represent the kinematic blocking by the wall. As a result, no viscous damping function is required in the k-ε-v2 model. This model can be thought of as a subset of a full second-moment closure in the sense that is analogous to the wall-normal Reynolds stress near to surfaces. The associated

redistribution term is obtained from the elliptic relaxation equation, which is a source in the $\overline{v^2}$-equation, as shown in Table 2. The k-ε model has some drawbacks in its application for flows with complex strain fields or significant body forces such as rotation, streamline curvature, swirling, and buoyancy. Under these conditions the individual Reynolds stresses are poorly represented by formula (4), even if the turbulent kinetic energy is computed within reasonable accuracy. The exact Reynolds stress transport equation on the other hand can account for the directional effects of the Reynolds stress field. The most complex and general RSM can account exactly for the turbulence production induced by shear, rotation, and stratification, and provides a better description than the eddy viscosity model. However, the RSM has some difficulties in modeling including turbulent diffusion (5d), dissipation tensor (5e), and pressure strain correlation (or redistribution term) (6).

One of the most important and difficult tasks in turbulence modeling is to model the pressure strain term. The RSM uses the local approach to model the pressure strain term. The local approach algebraically relates the unclosed redistribution term to the Reynolds stress anisotropy, mean strain, and vorticity tensors. This approach has been widely used for turbulence modeling, and all of the RANS models are based on this approach. Since these models are derived by quasi-homogeneous approximations, they require corrections by using damping functions, which are not universal to integrate the equation down to the solid boundaries. In order to avoid such problems, Durbin [10] introduced the so-called elliptic relaxation approach, which models directly the two-point correlation in the integral equation of the redistribution term using an isotropic exponential function. The redistribution term is no longer given by an algebraic relation, but rather by a differential equation. The non-local character is preserved through the elliptic operator and thus the model can be integrated down to the wall.

3. Assessment of the RANS Models

3.1. Channel Flow

The ideal flow for testing a near wall turbulence model is the two-dimensional channel flow. This flow is statistically homogeneous in the planes parallel to the walls, and hence the turbulence statistics are functions of the cross-stream coordinate y alone. A wealth of numerical and experimental data is available for this flow. Fig. 1 shows a schematic of the fully developed turbulent flow between two infinitely parallel plates. The mean-momentum equation from (1) can be written as

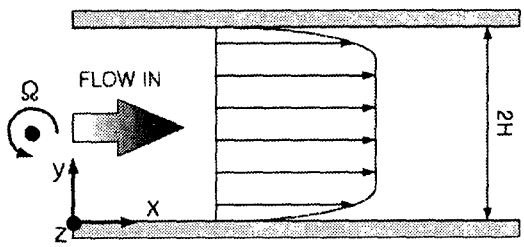

Fig. 1. Schematic of the Flow Configuration and Coordinate System for the Flat Plate Channel Flow

$$\frac{DU}{Dt} = -\frac{\partial P}{\partial x} + \frac{d}{dy}\left(\mu\frac{dU}{dy} - \rho\overline{u_1 u_2}\right) \qquad (9)$$

for a constant property fluid in a Cartesian coordinate system. P is the mean pressure. Since the velocity vector $U=(U(y), 0, 0)$ is aligned with the planes, the continuity constrain $\partial U_k/\partial x_k$ is automatically satisfied and $\partial P/\partial x$ becomes a constant. The unknown Reynolds stress can be

obtained from the eddy viscosity model (4) and the transport equation (5) governing the kinematic Reynolds stress tensor.

The momentum and Reynolds stress equations were solved by a semi-implicit, parabolic marching scheme. Marching converged to a steady-state solution when the sum of the absolute normalized mass residuals across the channel fell below 1e-10. These equations were also solved with a finite volume method, which uses the central differencing of the diffusive terms on a collocated grid. The calculations were carried out on a one-dimensional grid consisting of 326 cells (all the models except standard k-ε model using 40 cells) in the wall-normal (y) direction. The first grid point from the wall was situated at $y^+=0.25$. At the solid walls, no-slip boundary conditions were used together with $\overline{u_i u_i}$ and $\varepsilon = 2\nu k/y^2$ for the Reynolds stress and dissipation rate. The boundary conditions for f_{ij} are derived from the local solution of the model equation governing the wall-normal stress component, see Durbin (1993) for further details.

$$f_{11} = f_{33} = 0, \quad f_{22} = -20\nu^2\overline{v^2}/\epsilon y^4, \qquad f_{12} = -20\nu^2\overline{uv}/\epsilon y^4 \tag{10}$$

The mean velocities of seven RANS models are compared in Figs. 2 and 3. The mixing length model over predicts the DNS data in the near wall region, and the k-l model over predicts the DNS data in the center region. In general, the standard k-ε model predicts well in comparison with the other two models in the logarithmic layer. This predictive capability is enhanced by the use of the dissipation equation formulated partial differential equation.

The mean velocities of the low Reynolds number models are shown in Fig. 3. The RRSM under predicts the DNS data in the inner layer, but the other three models predict the DNS data with

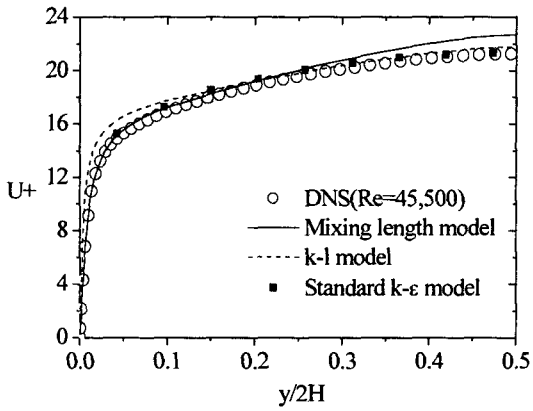

Fig. 2. Mean Velocities for Mixing Length, *k-l* and Standard *k-ε* Model in Channel Flow at Re_τ = 590

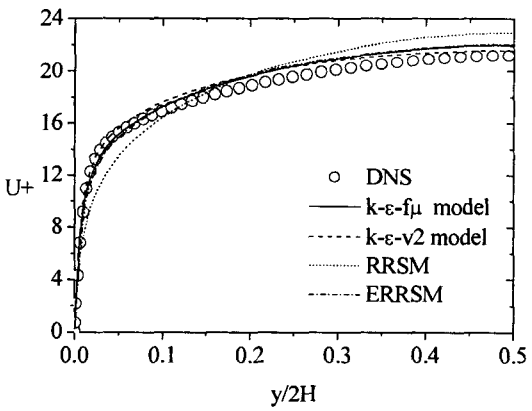

Fig. 3. Mean Velocities for *k-ε* Models and RSMs in Channel Flow at Re_τ = 590

good agreement. In the central region, the k-ε-v2 model is in good agreement with the DNS data, but ERRSM and k-ε-fμ slightly over predict the DNS data.

Fig. 4 shows a comparison of the turbulent kinetic energy of the two isotropic models (k-ε-fμ and k-ε-v2) and the two anisotropic models (RRSM and ERRSM). As shown in this figure, the ERRSM and k-ε-v2 predict the DNS data better than k-ε-fμ and RRSM in general. Fig. 5 shows the distribution of the normal stress components for

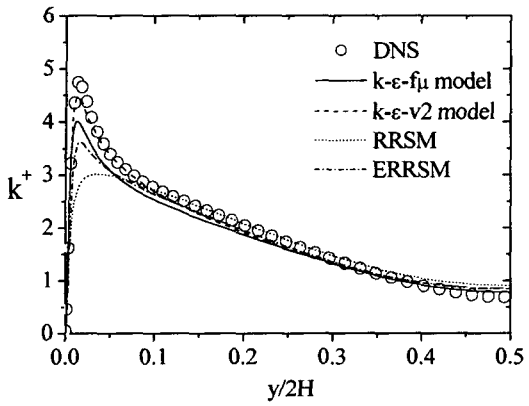

Fig. 4. Mean Velocities for *k-ε* Models and RSMs in Channel Flow at Re_τ = 590

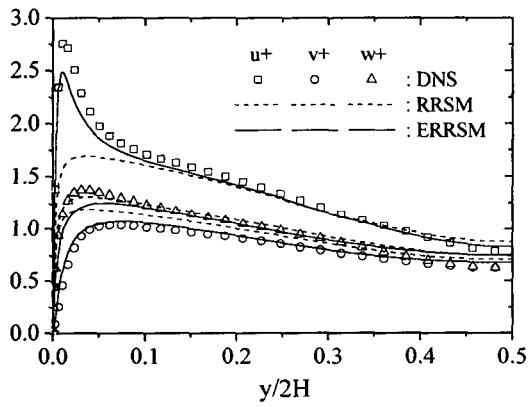

Fig. 5. Reynolds Stresses for RRSM and ERRSM in Channel Flow at Re_τ = 590

the RRSM and ERRSM. In the near wall region, the streamwise component u^+ of the RRSM was under predicted with the DNS data while the wall-normal component was over predicted. The ERRSM that uses the elliptic relaxation approach better predicts the Reynolds stress than RRSM in the near-wall region.

3.2. Channel Flow: Standard k-ε Model

The popularity of the standard k-ε model can be attributed to its computational efficiency and robustness at high Reynolds number flows. However, this model fails to yield a correct prediction of turbulent flows with streamline curvature in a non-circular channel or with respect to a rotating frame of reference. The standard k-ε model has been verified from several types of industrial application problems. In general, this model is known to have good prediction capability for wall friction and pressure drop in simple geometries with a coarse grid. However, the model does not necessarily always produce good results for any flow field, because of the geometrical dependence of the turbulence scale. It is important for this model to appropriately select the first grid point in view of the local equilibrium (P/ε=1), since the grid system influences the predictive capability of the flow fields. In this study, the turbulence effects for the first grid point and grid numbers were investigated. The boundary condition is obtained from the "row of the wall" assuming that the flow is in a local equilibrium. That is, the turbulent generation and dissipation rate are nearly equal in the log region.

Figs. 6 through 8 show the grid effects on the channel flow with the standard k-ε model. The analysis was performed by varying the grid numbers (N=8, 12, 20, 40) and the normalized distance of the first grid (y_1^+=25, 50, 100) from the wall. The streamwise velocity, kinetic energy, and dissipation profiles were calculated for the channel flow and compared with the DNS results [11].

Fig. 6(a) shows a comparison of the effects of the grid numbers for the first grid point y_1^+=25. The mean velocity is predicted fairly well for N=40. But the mean velocity is overestimated for N=8 and 12 at the center of the channel because of the error induced by the grid resolution to satisfy mass and momentum conservation. As shown in Figs. 6(b) and (c), the turbulent kinetic energy and the dissipation are poorly predicted,

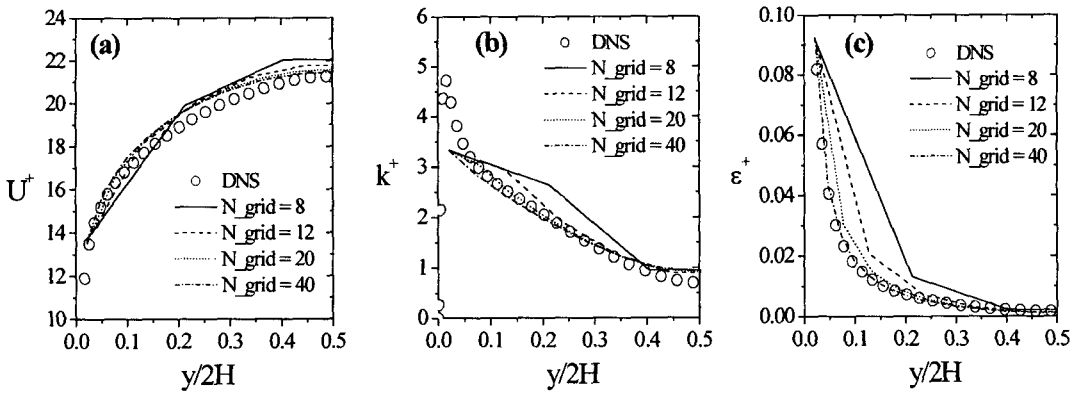

Fig. 6. Prediction of the Standard k-ε Model for the Grid Numbers at y_1^+ = 25 (a) Mean Velocity (b) Turbulent Kinetic Energy (c) Dissipation Rate

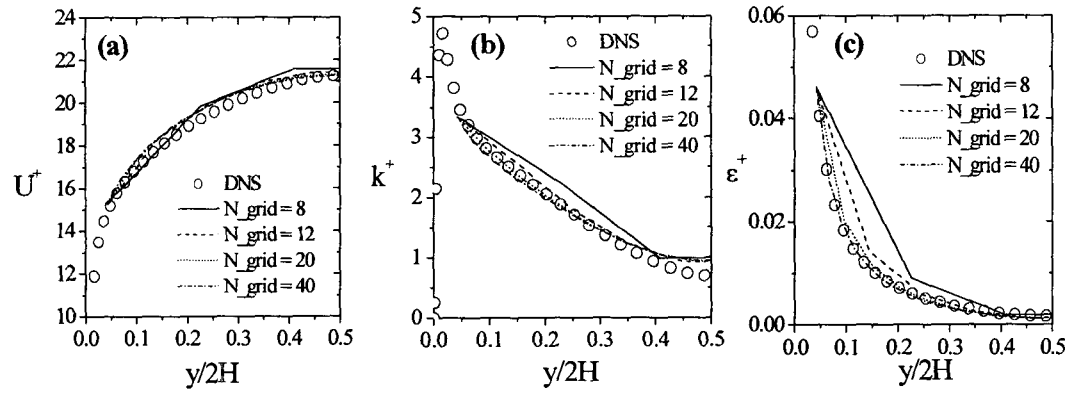

Fig. 7. Prediction of the Standard k-ε Model for the Grid Numbers at y_1^+ = 50 (a) Mean Velocity (b) Turbulent Kinetic Energy (c) Dissipation Rate

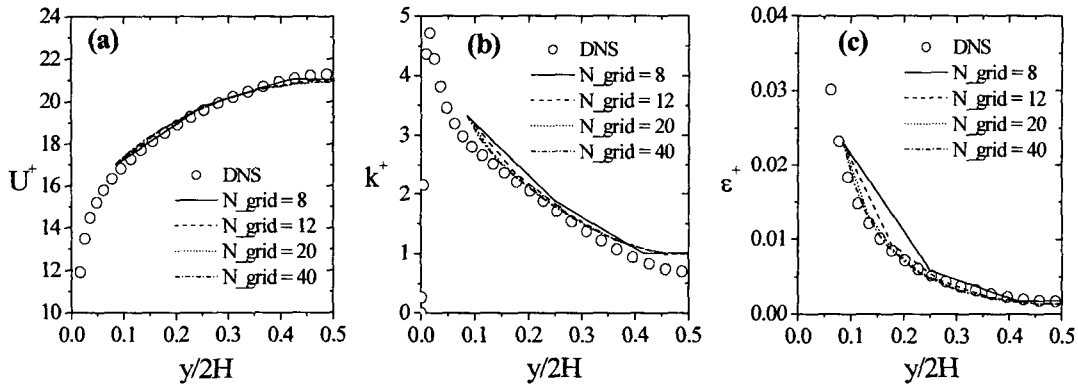

Fig. 8. Prediction of the Standard k-ε Model for the Grid Numbers at y_1^+ = 100 (a) Mean Velocity (b) Turbulent Kinetic Energy (c) Dissipation Rate

since the turbulent generation is greater than the dissipation at the first grid point of $y_1^+ = 25$.

For the grid of $y_1^+ = 50$, the results show a better estimation than the grid of $y_1^+ = 25$ for all the turbulent qualities, as shown in Fig. 7. In spite of the use of the same number of grids, the result shows a better prediction due to the fitting location of the first grid point. Fig. 8 presents the results for the grid of $y_1^+ = 100$. In this case, all the turbulent quantities U^+, k^+ and ε^+ are overestimated for the DNS data in the logarithmic layer because the streamwise velocity between the wall boundary condition and the first grid point is calculated linearly. However, this error is relatively decreased with an increase of the Reynolds number.

3.3. Rotating Channel Flow

Flows in the rotating frames of reference are encountered in a variety of applications, for example, in rotating devices such as turbines, pumps, compressors, and centrifuges. This flow is useful to investigate the anisotropy behavior of the Reynolds stress for asymmetric flows. The effects of rotation on the Reynolds stress are included through rotational terms (5b) and the rapid-pressure-strain correlation (6), which appears in the transport equations governing the Reynolds stress tensor. It is important to distinguish between these two contributions because the production tensor often appears in the closure models.

Fig. 1 shows a schematic of the fully developed turbulent flow between two infinitely parallel plates in a spanwise rotation with a constant angular velocity $\Omega=(0, 0, \Omega)$ about the z-axis. The x- and y-momentum equations can be written as

$$\frac{DU}{Dt} = -\frac{\partial P^*}{\partial x} + \frac{d}{dy}\left(\mu\frac{dU}{dy} - \rho\overline{u_1 u_2}\right) \quad (11)$$

$$0 = -\frac{\partial P^*}{\partial y} - 2\rho\Omega U - \frac{d}{dy}\left(\rho\overline{u_2 u_2}\right) \quad (12)$$

P^* denotes the mean reduced pressure $P^* = P - 1/2\rho\Omega^2(x^2+y^2)$. The only direct effect of the system rotation is the Coriolis force $-2\Omega U$, which acts in the negative y-direction and according to (12) balances the pressure force $-\partial P^*/\partial y$ and the net turbulence force $-d(\rho\overline{u_2 u_2})/dy$. It should moreover be observed that the influence of the centrifugal force is completely absorbed in the reduced pressure P^*. The unknown Reynolds stress and dissipation rate can be obtained from (3) and (5).

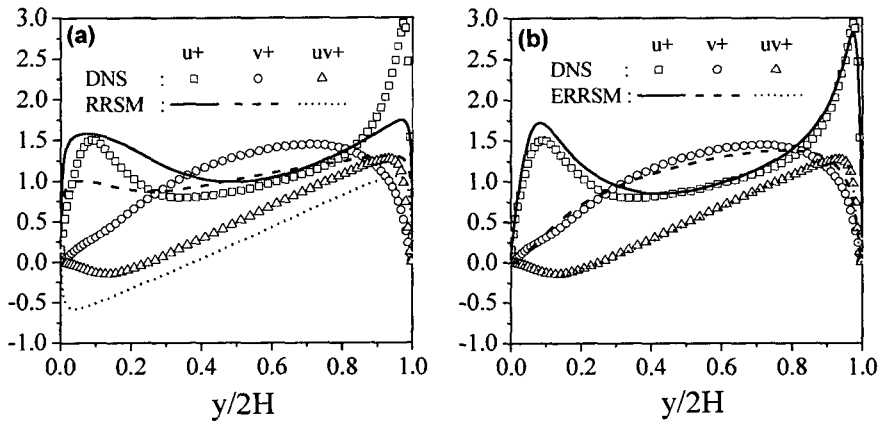

Fig. 9. Reynolds Stresses in the Rotating Channel (Ro=0.2) for (a) RRSM (b) ERRSM

Fig. 9 compares the predicted Reynolds stress distributions of the channel cross-section with the DNS data [12]. The peak of the streamwise components is nicely captured by ERRSM and the other stress components u^+ agree well with the DNS data in comparison with RRSM. ERRSM better predicts the capture of relaminarization in the suction side (y=0) of the channel. The poor prediction of the RRSM is considered to be due to an increase in the pressure strain at the near-wall region. The eddy viscosity models are not investigated because the rotating term (5b) is zero in a fully developed channel flow. Also, note that the models such as the non-linear k-ε and ASM (algebraic stress model) are indirectly affected by the eddy viscosity and the algebraic Reynolds stress.

3.4. Square Sectioned U-Bend Duct Flow

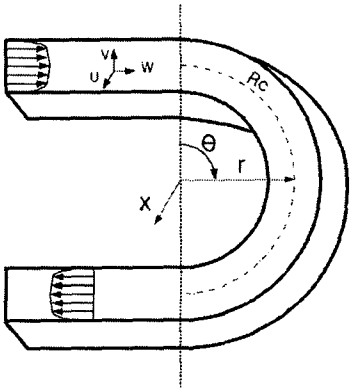

Fig. 10. Geometry and Coordinate System for Square Sectioned U-Bend Duct Flow

Table 3. Flow Conditions of Square Sectioned U-Bend Duct

Reynolds Number	Dean Number	Hydraulic diameter(m)	Curvature ratio
$\frac{DU_B}{\nu}$	$Re\sqrt{\frac{D}{R}}$	$\frac{4A}{P}$	$\frac{Rc}{D}$
56,690	30,940	0.0889	3.357

The turbulent flow field through a passage with a curvature has been one of primary interest in fluid engineering. Owing to the curvature, pressure induced secondary motions have significant consequences in the turbulent strain field. Chang et al. [14] and Lee et al. [15] investigated this type of turbulent flow using LDV and hotwire devices in a square sectioned U-bend duct flow with a curvature ratio of Rc/D=3.357. The experimental data showed an existence of "camel back" shapes in the streamline velocity distribution of the curvature section. They reported that these characteristic profiles were the result of strong secondary flow motions.

As illustrated in Fig. 10, the U-bend duct flow with the curvature ratio Rc/D=3.357 is discussed to assess the model performance. The computer program used is the semi-elliptic code (parabolic marching for θ-direction) in an orthogonal-cylindrical coordinate system developed by Chun et al. [13]. The SIMPLER algorithm provides a method of calculating pressure and velocities. It uses the QUICK scheme for the convection terms of the momentum equations while the Hybrid differencing scheme is applied for Reynolds stress, dissipation, and elliptic relaxation equations. The computation grids used extend up to the symmetry plane and consist of $52(x) \times 100(r) \times 156(\theta)$ (with 5D inlet and 10D outlet tangents) nodes. This program uses a staggered grid for the velocity and Reynolds stress components. Separate computations of the fully developed straight duct flows have been performed in order to provide the inlet conditions.

In this study, assessments of the curvature effects were conducted for three turbulent models, Launder and Sharma' s k-ε-fμ model [7], Speziale et al.' s RSM [9], and Durbin' s elliptic relaxation model [10] for the flow of a square sectioned U-bend duct flow. Fig. 11 shows a comparison of the predicted streamwise mean velocity distribution

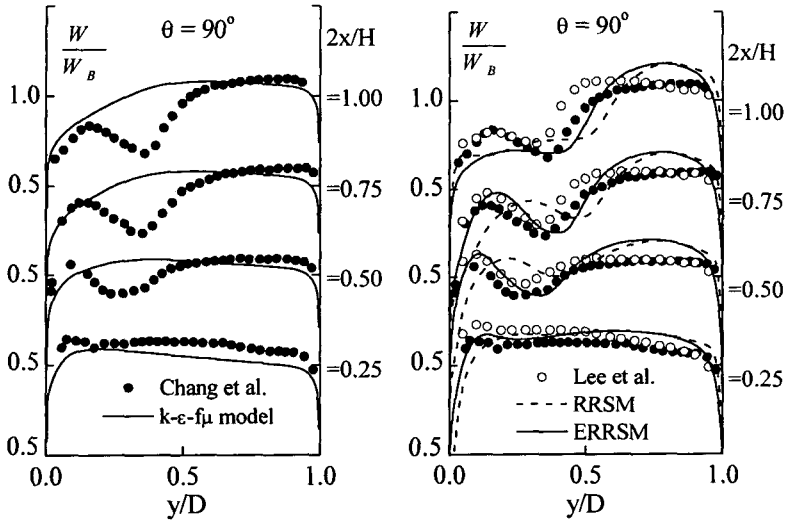

Fig. 11. Streamwise Mean Velocity Profiles in the U-Curved Duct Flow at θ = 90

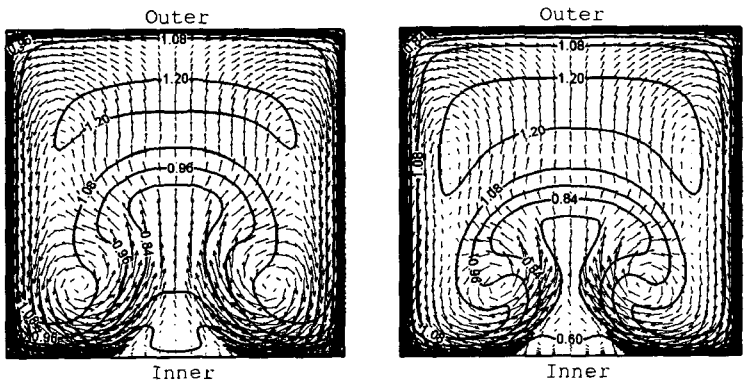

(a) RRSM **(b) ERRSM**

Fig. 12. Secondary Flow Vectors and Streamwise Mean Velocity Contours at θ = 90

with the experimental data of Chang et al. and Lee et al. at the streamwise section of θ=90 for Re=56,690. The symmetry plane corresponds to 2x/H=1.0 and the velocity distributions at 2x/H=0.25, 0.5, 0.75 and 1.0 are compared. Both RRSM and ERRSM successfully reproduce the appearance of the camel back shapes in the velocity distribution. However, the dip-velocity profiles of RRSM are shifted toward the outside (y/D=1.0) in comparison with the experimental data. The k-ε-fμ model does not predict these shapes. Although the agreement of the predictions and experiments is not perfect, ERRSM generally reproduces well the characteristic velocity distribution of the experiments. These shapes are the results of loss of streamwise momentum due to the secondary flow forming a strong downward motion from the symmetry plane to the bottom wall. Fig. 12 shows the streamline velocity contours and secondary velocity vectors for the

same section. The velocity contours of "mushroom shape" appear in the inner wall region due to the strong secondary flow. This phenomenon is closely related to the curvature effect and the pressure drop between the inner wall and outer wall.

4. Results and Discussions

The existing turbulence models were assessed for application to a three dimensional flow analysis of the SMART primary coolant system for a non-rotating and rotating channel flow, square sectioned U-bend duct flow, and other references. The models were evaluated in terms of theorization, economical efficiency, applicability, and accuracy, as shown in Table 4. The results are numerically scaled as 1 to 5. That is, 1=poor, 2=moderate, 3=good, 4=fair, and 5=excellent.

The aspect of theorization is evaluated based on the degree of representation of the physical phenomena and the theoretical basis of the models. The mixing length and k-l models are given a low score in theorization due to the uncertain characteristic length scale. The standard k-ϵ model merits a high score due to the complete characteristic length and velocity scales, which require only boundary conditions. RSMs are found to have a low score in comparison with the k-ϵ type models, since the pressure strain term in the Reynolds equation is not modeled with an accurate approach as of yet. If the pressure strain is modeled theoretically, RSM may be considered a better model than the eddy viscosity model. ERRSM is evaluated as a better model than RRSM because the pressure strain term was derived through a better theoretical approach than that of the RRSM. Also, the ERRSM and the k-ϵ-v2 model, which are free from the damping function, have better scores than the RRSM and the k-ϵ-fμ model.

Applicability is related to the use of the wall functions and ad hoc damping functions shown in Table 2. Generally, damping functions are introduced to extend the models down to the wall. However, the reproduction of the near wall behavior of turbulence using the complex correction terms loses some consistency, as the basic assumptions are not valid in this region. The elliptic relaxation approach is based on theoretical analysis and simple modeling of the two-point correlations involved in the integral form of the distribution term. While it is difficult to define y^+ and Uτ for complex geometry in the standard k-ϵ model, the models based on the elliptic approach, ERRSM and k-ϵ-v2, have been successfully applied in a number of different situations. Therefore, the turbulence models with the wall-correction

Table 4. Assenssment of Applicable Turbulent Models for the Integral Type Reactor SMART

Model	Theorization	Application	Economy	Accuracy	Average
MLM	1	3	4	2	2.50
k	2	2	4	2	2.50
k-ε	4	4	5	3	4.00
k-ε-f_μ	3	3	3	4	3.25
k-ε-v^2	4	5	4	5	4.50
RRSM	3	3	3	3	3.00
ERRSM	4	5	3	5	4.25

Table 5. Comparison of the Selected Turbulent Models

Model	Advantages	Disadvantages
$k-\varepsilon-\overline{v^2}$	• Isotropy, low Reynolds number model. • The non-local effects in the turbulent boundary layers. • The most excellent low Reynolds number model for the 3-D analysis of the SMART primary coolant system. • No dependence on the distance from the wall. • No damping functions or wall functions to adjust the behaviour of turbulent quantities.	• Typically 20% more computational time than the low Reynolds k-ε models. • Isotropic model for the k and ε equations. • Poor performance for the curved boundary layers, swirling, rotating flows, and buoyancy flows.
$k-\varepsilon$	• Isotropy, high Reynolds number model. • Simplest turbulent model for which only boundary conditions need to be supplied. • Well established and the most widely validated turbulent model. • The good predictive capability for general features such as pressure drop, wall friction in three dimensional turbulent flows. • To assess easily high Reynolds number flows by economic costs.	• No prediction in the near wall. • Dependence on the distance from the wall. • Isotropic model of the k and ε equations. • Poor performance for the curved boundary layers, swirling, rotating flows, and buoyancy flows.
ERRSM	• Strong inhomogeneity and anisotropic effects, low Reynolds number non-local model. • The most general RANS model. • Useful thermal-hydraulic design tool of the components such as main coolant pump, steam generator. • Excellent performance for the complex geometries. • Included exact shear, rotation and buoyancy production rate in Reynolds stress equations.	• Very large computing costs(six extra Reynolds stress equations and six extra elliptic relaxation equations). • Not as widely validated as the k-ε models. • Performs just as poorly as the k-ε model in some geometries. • Difficulties in modeling for the pressure strain correlation, dissipation tensor and turbulent diffusion.

functions, such as the wall functions and damping functions, should be carefully introduced to the flow fields of the SMART primary coolant system.

Economical efficiency is the criteria related to the time cost of the computation. The SMART primary coolant system flows with a high Reynolds number and requires a large number of grids to solve the flow fields due to the inclusion of multi-blocks and multi-walls. For this condition the most economic model is the standard k-ε model because it does not require a grid at the near-wall region. Although the k-ε-v2 model uses one more equation than the k-ε-fμ model, the k-ε-v2 model has a better score than the k-ε-fμ model due to the numerical stability obtained from the monuse of the wall topography parameters such as the damping functions and the geometrical parameters are used.

Accuracy denotes the prediction capability of the tested flow fields. For a channel flow without a body force, the k-ε-v2 model shows that the turbulent kinetic energy and streamwise velocity are in very good agreement with the DNS data. ERRSM in the rotating channel flows better predicts the capture of relaminarization in the suction side of the channel in comparison with RRSM. In a three-dimensional U-bend duct flow, the ERRSM successfully predicts the streamwise velocity and secondary flow in comparison with RRSM and the k-ε-fμ model.

5. Conclusions

Assessments of turbulence models were conducted on the RANS models that will be implemented into the computer code TASS-3D, which has been developed for a three-dimensional flow analysis of the SMART primary coolant system. Seven RANS models are investigated. Among these, three models (k-ε, k-ε-v2 and ERRSM) to be implemented into TASS-3D were selected with consideration of economical efficiency, accuracy, theorization, and applicability to the complex three-dimensional flow analysis of the SMART primary coolant system. A summary of the three models selected is given in Table 5.

The standard k-ε model, the k-ε-v2 model, and the ERRSM are selected based on the results of benchmarking calculations for channel flow, rotating channel flow, square sectioned U-bend duct flow, and relevant references. In the log layer, the standard k-ε model better predicted the channel flow in comparison with the mixing length and other eddy viscosity models despite the use of small grid numbers. The k-ε-v2 model and ERRSM have the advantage of applicability to complex geometries. The k-ε-v2 model and ERRSM are free from damping function and distance from the wall, and show better predictions for a strong inhomogeneous flow field in near wall flows.

References

1. KAERI/TR-2142/2002, Basic Design Report of SMART, KAERI,(2002).
2. KAERI/TR-2540/2003, Development of Inhomogeneous k-ε-v2 Turbulence model for 3D Flow Analysis of SMART-P, KAERI,(2003).
3. E. R. Van Driest, "On Turbulent Flow Near Wall," Journal of the Aeronautical Sciences, Vol.23, p.1007(1956).
4. M. P. Escudier, "The Distribution of Mixing Length in Turbulent Flows Near Wall," Imperical College, Heat Transfer Section Report SF/R/2(1966).
5. M. Wolfshtein, "Convection Processes in Turbulent Impinging Jets," Imperial College, Heat Transfer Section Report SF/R/2(1967).
6. B. E. Launder, and D. B. Spalding, "The Numerical Computation of Turbulent Flows," Comput. Methods Appl. Mech. Eng., Vol.3, pp.269-289(1974).
7. B. E. Launder and B. I. Sharma, "Application of the Energy Dissipation Model of Turbulence to the Calculation of Flow Near a Spinning Disc," Letters in Heat and Mass Transfer, Vol.1, No.2, pp.131-138(1974).
8. P. A. Durbin, "Near wall turbulence closure modeling without damping function," Theoret. Comput. Fluid Dyn. Vol.3, pp.1-13(1991).
9. C. G. Speziale, S. Sarkar, & T. B. Gatski, "Modeling the pressure strain correlation of turbulence : an invariant dynamical system approach," J. Fluid Mech. 227, pp.245-272(1991).
10. P. A. Durbin, "A Reynolds stress model for near-wall turbulence," J. Fluid Mechanics, Vol.249, pp.465-498(1993).
11. R. D. Moser, J. Kim, and N. N. Mansour, "Direct numerical simulation of turbulent

channel flow up to Re_τ," Phys. Fluids, Vol.11, pp.943-948(1999).

12. R. Kristoffersen and H.I. Andersson, "Direct simulations of low-Reynolds-number turbulent flow in a rotating channel," J. Fluid Mech. 177, pp.133-166(1993).
13. K. H. Chun, Y. D. Choi and J. K. Shin, "Developing Turbulent Heat Transfer in a 360 Bend of Square cross section," Heat Transfer-Asian Research, 28(2), p.77(1999).
14. S. M. Chang, J. A. C. Humphrey and A. Modavi, "Turbulent flow in a strongly curved U-bend and downstream tangent of square cross sections," PCH Phys. Chem. Hydrodynamics, 4, p.243(1983).
15. G. H. Lee, Y. D. Choi, and S. K. Cho, "Measurement of turbulent flows in a square sectioned 270 degree bend," Proceedings of the KSME 2000 Fall Annual Meeting B. pp.467-472(2000).